









RESEARCH ARTICLE | OCTOBER 05 2023

Comparative quantum chemical and spectral characterization of meso-tetra(4-sulfonatophenyl) porphine forms as seeds for J- and H-aggregates

Laura Baliulyte  ; Darius Abramavicius  ; Saulius Bagdonas  ; Agne Kalnaityte  ; Vilius Poderys  ; Ricardas Rotomskis  ; Virginijus Barzda  



AIP Advances 13, 105011 (2023)

<https://doi.org/10.1063/5.0167120>



CrossMark

Articles You May Be Interested In

Completing the dark matter solutions in degenerate Kaluza-Klein theory

J. Math. Phys. (April 2019)

Gibbs measures based on 1d (an)harmonic oscillators as mean-field limits

J. Math. Phys. (April 2018)

An upper diameter bound for compact Ricci solitons with application to the Hitchin–Thorpe inequality. II

J. Math. Phys. (April 2018)

AIP Advances

Why Publish With Us?



25 DAYS
average time
to 1st decision



740+ DOWNLOADS
average per article



INCLUSIVE
scope

[Learn More](#)



Comparative quantum chemical and spectral characterization of meso-tetra(4-sulfonatophenyl) porphine forms as seeds for J- and H-aggregates

Cite as: AIP Advances 13, 105011 (2023); doi: 10.1063/5.0167120

Submitted: 18 July 2023 • Accepted: 12 September 2023 •

Published Online: 5 October 2023



View Online



Export Citation



CrossMark

Laura Baliulyte,^{1,2}  Darius Abramavicius,^{1,2}  Saulius Bagdonas,¹  Agne Kalnaityte,¹  Vilius Poderys,³ 
Ricardas Rotomskis,^{1,3}  and Virginijus Barzda^{1,4,5,a)} 

AFFILIATIONS

¹Laser Research Center, Faculty of Physics, Vilnius University, Sauletekio Ave. 9, LT-10222 Vilnius, Lithuania

²Institute of Chemical Physics, Faculty of Physics, Vilnius University, Sauletekio Ave. 9, LT-10222 Vilnius, Lithuania

³Biomedical Physics Laboratory, National Cancer Institute, P. Baublio Str. 3b, LT-08406 Vilnius, Lithuania

⁴Department of Chemical and Physical Sciences, University of Toronto Mississauga, 3359 Mississauga Rd., Mississauga, Ontario L5L 1C6, Canada

⁵Department of Physics, University of Toronto, 60 St. George St. Toronto, Toronto, Ontario M5S 1A7, Canada

^{a)} Author to whom correspondence should be addressed: virgis.barzda@utoronto.ca

ABSTRACT

Aggregation of 5,10,15,20-tetrakis(4-sulfonatophenyl) porphyrin (TPPS₄) molecules as a function of solvent pH is a complex process because of the co-existence of many possible interacting monomeric ionic forms that self-assemble into various aggregate structures. Possible seeding elements of aggregates were studied using quantum chemical calculations based on density functional theory to determine favorable ionic forms and their dimers, and the simulated spectral characteristics were compared with the measured absorption spectra. Five different forms of TPPS₄ monomers and ten dimers were found as possible candidates for aggregate precursors. It was found that monomeric forms dominate at pH = 12.1, pH = 7.1, pH = 4.1, and pH = 3.0 as well as at pH = -1.0. In contrast, J-type dimers become a dominant form at pH = 1.0.

© 2023 Author(s). All article content, except where otherwise noted, is licensed under a Creative Commons Attribution (CC BY) license (<http://creativecommons.org/licenses/by/4.0/>). <https://doi.org/10.1063/5.0167120>

INTRODUCTION

In the past few decades, water-soluble, metal-free 5,10,15,20-tetrakis(4-sulfonatophenyl) porphyrin (TPPS₄) and its various derivatives have been extensively studied for applications in photodynamic therapy (PDT)¹ and optoelectronics.² The monomers of TPPS₄ efficiently self-associate into large J-aggregates (side-by-side) or H-aggregates (face-to-face) in aqueous media depending on the concentration of TPPS₄ molecules and pH value of the solution.^{3–5} TPPS₄ aggregates are important theranostic agents for photo-thermal therapy (PTT) and photoacoustic imaging (PAI) due to high efficiency conversion of light energy into heat⁶ because of the intense absorption in the phototherapeutic window. The aggregation of TPPS₄ results in various structural forms, which can interact with each other, forming peculiar supramolecular aggregates.⁷ The aggregation process is complex and not fully understood, in

particular, with respect to the types of aggregates that can form under various aggregation conditions.

TPPS₄ belongs to the class of porphyrins that are organic cyclic compounds formed by the linkage of four pyrrole rings through methine bridges.⁸ The structure of porphyrin is based on the unsubstituted ring of porphine.⁹ It contains 18 π electrons along the main (shortest) cyclic pathway and meets Hückel's $4n+2$ rule for aromatic systems. This aromatic nature explains the intense color of porphyrins. Many different functional groups can be substituted onto porphine macrocycles at the β -position or the meso-position.⁸

Various porphyrin compounds are classified according to several factors e.g., the presence or absence of metal-ions at the center of the molecule (a porphine or a metalloporphyrin),¹⁰ overall molecular charge properties (cationic, anionic, or neutral),¹¹ and the type of side groups that determine water solubility (lipophilic, amphiphilic, or hydrophilic).¹² The dominant form of TPPS₄ depends on the pH

of the solvent: $H_2TPPS_4^{4-}$ dominates in alkaline ($pH \approx 12$) and neutral solutions ($pH \approx 7$), $H_4TPPS_4^{2-}$ dominates in a pH range of $\approx 4-3$, $H_6TPPS_4^0$ is prevalent at a pH of ≈ 1 , and $H_8TPPS_4^{2+}$ appears to dominate at even lower pH .¹³⁻¹⁵ The chemical structures of these $TPPS_4$ forms are shown in Fig. 1. The presence of different ionic forms leads to the formation of various dimers that further assemble into different aggregate structures.

To date, only small J-aggregate structures of $TPPS_4$ have been studied using theoretical calculations: H_4TPPS_4 J-dimers were determined by Becke's three-parameter hybrid functional applying the non-local correlation provided by the Lee, Yang, and Parr (B3LYP) method, which is a representative of standard density functional theory (DFT), along with the Pople 6-31G* basis set. It has been

determined that H_4TPPS_4 J-dimers could have parallel (achiral), left-handed helical, or right-handed helical structures.¹⁶ Aggregated structures have also been predicted according to the constituent monomeric structures. Based on theoretical calculations, Augulis *et al.* suggested that the zwitterionic $TPPS_4$ structure is asymmetric, which self-assembles into a bent thread, that can contain ~ 60 monomers in a loop. It leads to a loop diameter of about 20 nm.¹⁷ Other studies qualitatively predicted structures of aggregates by analyzing x-ray scattering or diffraction data. Gandini *et al.* simulated the cylinder model based on the small angle x-ray scattering (SAXS) data at 4.0 pH. The authors suggested that ~ 26 porphyrin molecules are present in a single ring while ~ 3000 H_4TPPS_4 molecules are contained in the whole nanocylinder.¹⁸

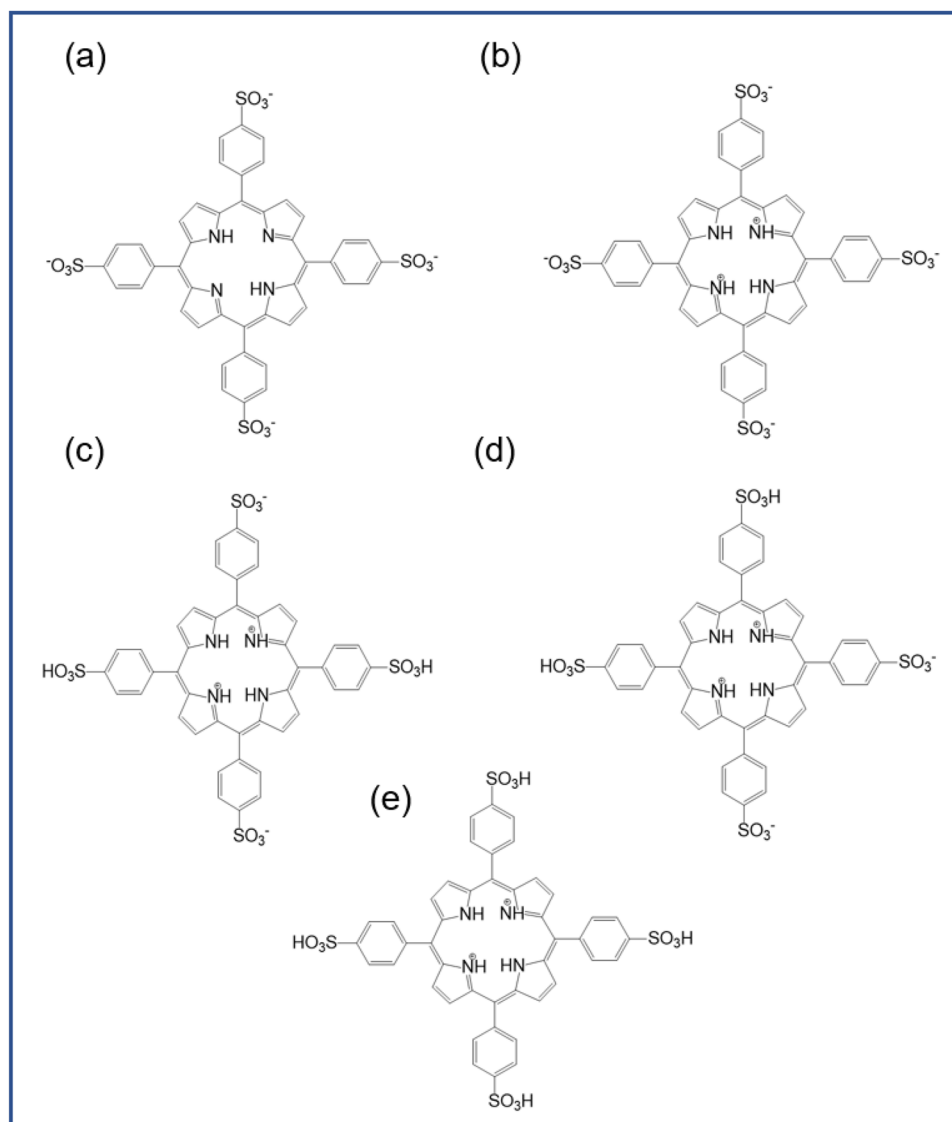


FIG. 1. Chemical structures of the $TPPS_4$ monomers. (a) $H_2TPPS_4^{4-}$ (tetra-anion form), (b) $H_4TPPS_4^{2-}$ (diacid form), (c) $H_6TPPS_4^0$ [Z1 (zwitterionic form); SO_3H groups are opposite], (d) $H_6TPPS_4^0$ [Z2 (zwitterionic form); SO_3H groups are adjacent], and (e) $H_8TPPS_4^{2+}$ (dication form).

Friesen *et al.* proposed that $H_4TPPS_4^{2-}$ molecules first assemble into ~6-nm diameter rings. These rings are envisioned to be cyclic N-mers. They suggest that the N-mers consist of 10–16 molecules in a ring. Then rings assemble into helical nanotubes.¹⁹ The model is supported by x-ray diffraction of protonated tetraphenylporphine (H_2TPP).²⁰ However, these studies did not suggest an aggregate structure at the molecular level.

The aggregation state of $TPPS_4$ molecules can be related to changes in spectral properties of the samples. It is widely accepted that H-aggregates are characterized by a blue-shifted (hypsochromic) absorption band while J-aggregates possess a red-shifted (bathochromic) absorption band with respect to the monomer B (Soret) absorption band.²¹ The linear dichroism of the B band and absorption spectra of zwitterionic $TPPS_4$ were simulated by including resonant excitonic couplings.²² Stradomska and Knoester additionally included vibronic effects and the coupling between the B and Q bands. The obtained spectra (B and Q bands) could be used for a more detailed interpretation of the structure of $TPPS_4$ aggregates.²³ Valanciunaite *et al.* investigated the influence of bovine serum albumin (BSA) on the formation of J-aggregates of $TPPS_4$ at pH = 1.3 using fluorescence and absorption spectroscopy and showed that the combined interaction of protonated $TPPS_4$ monomers within J-aggregates is stronger than the interaction with BSA.²⁴ Correa *et al.* determined that changing the medium from water to micelle does not greatly affect the absorption spectra for non-protonated $TPPS_4$. These results indicate a weak interaction of the $TPPS_4$ porphyrin ring π - π system with the environment. They also noticed that bi-protonation of this molecule induces significant changes in the nonlinear optical properties of $TPPS_4$ and associated those changes with the difference in the symmetry of molecules before and after excitation.²⁵

To understand the structure and formation process of $TPPS_4$ J- and H-aggregates, it is important to know the initial seed-structures and elementary units (dimers) that constitute the aggregates. In this paper, solutions of low concentration $TPPS_4$ molecules are characterized by absorption spectroscopy in a wide range of pH values where only monomers and possibly dimers of $TPPS_4$ are expected to be present. $H_2TPPS_4^{4-}$ (tetra-anion form [Fig. 1(a)]), $H_4TPPS_4^{2-}$ (diacid form [Fig. 1(b)]), $H_6TPPS_4^0$ (zwitterionic form [Figs. 1(c) and 1(d)]) and $H_8TPPS_4^{2+}$ (dication form [Fig. 1(e)]) monomers and their J- and H-dimers are characterized by quantum chemistry calculations. According to previous studies, the expected chemical structures as a function of pH are known: tetra-anion form corresponds to pH > 6, diacid forms are typical for the pH range of 3–4, zwitterionic form is expected at a pH of ≈ 1 , while all four sulfonic groups of $TPPS_4$ are protonated at pH < 1.^{13–15,26–28} However, possible aggregation and molecular packing is not known.

In this study, the modeled seed-structures are compared with spectroscopic measurements. The comparative study of modeled and experimental spectra provides information about the likely aggregation process taking place under different conditions, and allows to predict the structure of the selected aggregates.

MATERIALS AND METHODS

$TPPS_4$ [as meso-tetra(4-sulfonatophenyl) porphine dihydrochloride powder] was purchased from Frontier Scientific Inc.,

USA. Hydrochloric acid (37% aqueous solution) and sodium hydroxide (in solid form) were purchased from Honeywell International Inc., USA. All reagents were used without further purification. The stock solution ($c = 10^{-3}$ mol/l) was prepared by dissolving $TPPS_4$ powder in deionized water. To make $TPPS_4$ solutions for experiments, first, aqueous solutions of required pH were prepared by titrating deionized water with 1M sodium hydroxide aqueous solution (pH = 12.1), with 0.1M and 1M hydrochloric acid (pH = 3.0 and pH = 1.0, respectively) or with both HCl and NaOH solutions (pH = 7.1 and pH = 4.1, respectively). The pH value of the solutions was measured using an inoLab 720 pH-meter (Xylem Inc., USA) with a SenTix Mic glass electrode. $TPPS_4$ solutions were made by adding small volumes (30 μ l) of the $TPPS_4$ stock solution ($c = 10^{-3}$ mol/l) into the prepared aqueous solutions of different pH values. For preparation of pH = -1.0 solution, a small volume (30 μ l) of the $TPPS_4$ stock solution was diluted with concentrated (37%) hydrochloric acid. The final concentration of $TPPS_4$ in all prepared solutions was $c = 3 \cdot 10^{-6}$ mol/l.

The steady state absorption spectra of $TPPS_4$ solutions were measured using a Varian Cary 50 UV-visible absorption spectrometer (Varian Inc., Australia). The spectral resolution of the measured spectra was <1.5 nm. Measurements were performed in polystyrene cuvettes with a 1 cm optical path. The absorption spectra of $TPPS_4$ solutions were recorded at different pH values ranging between -1.0 and 12.1.

Structures of $TPPS_4$ monomers and dimers were theoretically analyzed using DFT with the Coulomb-attenuating “Becke 3-parameter Lee–Yang–Parr” functional (CAM-B3LYP) and Pople 6-31G(d,p) basis set. Electrostatic interactions and hydrogen bonds between the positively charged porphyrin ring and negatively charged sulfonate groups (SO_3^-) are very important for dimer formation. In addition, π - π interactions play a large role in porphyrin dimerization.²⁹ It is well known that CAM-B3LYP combines the hybrid qualities of B3LYP and the long-range Coulomb correction.³⁰ For calculation of absorption spectra, the time-dependent density functional theory (TDDFT) with CAM-B3LYP/6-31G(d,p) was used to calculate the excited state properties, such as transition energies and oscillator strengths. The polarizable continuum model (PCM) was used to approximately evaluate the influence of the solvent (water).³¹ Chemical structures were visualized using ChemDraw 20.0 and GaussView 6.1³² programs. The Gaussian 16 C.01³³ software was used for the calculations.

The strategy of theoretical calculations was as follows: First, the geometry of the $TPPS_4$ monomers— $H_2TPPS_4^{4-}$ (tetra-anion form [Fig. 1(a)]), $H_4TPPS_4^{2-}$ (diacid form [Fig. 1(b)]), two types of $H_6TPPS_4^0$ (zwitterionic form [Figs. 1(c) and 1(d)]) and $H_8TPPS_4^{2+}$ (dication form [Fig. 1(e)])—was optimized. The superscript denotes the total charge of the structure. In addition, two different types of the zwitterionic form of the $TPPS_4$ molecules were considered with respect to two SO_3^- ionized groups: either opposite (Z1 monomer) or adjacent (Z2 monomer) SO_3^- groups of the $TPPS_4$ molecule.

Optimized monomeric structures were used to construct the dimers. Two different types of dimers were considered. We denote them as J-dimers and H-dimers, reflecting different molecular packing.³⁴ The J-dimer is defined as a structure where one SO_3 group of one molecule is positioned on the top of the central part of the other molecule. Different J-dimers are obtained when one of the

molecules (being shifted aside) is additionally rotated. In order to obtain all possible J-dimers, one monomer can be rotated in steps of 90° . Hence, we could obtain at most four types of J-dimers where one monomer is rotated by 0° , 90° , 180° , and 270° and the second monomer remains fixed. Electrostatic interactions between the negatively charged sulfonate groups and the positively charged porphyrin ring are usually considered the most essential factors for J-dimer formation. For this reason, we consider only this type of J-dimers. Accordingly, different configurations of J-dimers can be formed out of Z1 and Z2 monomers. Other forms are obtained when all four end-groups are the same, namely, $H_4TPPS_4^{2-}$ (four SO_3^-) and $H_8TPPS_4^{2+}$ (four SO_3H).

H-dimer is defined as a structure where one molecule is positioned directly on top of the other without shifting (a sandwich configuration). For H-dimers, the molecules are not coordinated by sulfur atoms, so the monomers are either not rotated with respect to each other or one of the monomers is rotated in steps of 45° . Overall, in this manner, it is possible to define a single J- and two H-dimers of $H_4TPPS_4^{2-}$, six J- and four H-dimer configurations of $H_6TPPS_4^0$, and two H-dimers of $H_8TPPS_4^{2+}$. Notice the dominance of each ionic form—a tetra-anion, diacid, zwitterionic, and dication—correspond to different values of pH of the solvent.^{13,35} Different monomers of all four (tetra-anion, diacid, zwitterionic, and dication) ionic forms (with corresponding dimers) were considered separately. All 16 initial configurations are presented in the supplementary material (Fig. S1).

Geometry optimization was performed using the CAM-B3LYP method for all 16 dimers described above. Only 10 out of the 16 dimers converged (in terms of energy minimization) into stable structures. To verify the convergence results, the calculations were repeated using the Minnesota functional (M06-2X), which rendered the same final results. M06-2X was chosen due to its suitability

for studying noncovalent interactions.³⁶ Only the converged $TPPS_4$ dimers are described in the article.

RESULTS

Structural analysis based on DFT

Structures based on the $H_2TPPS_4^{4-}$ monomer

In the $H_2TPPS_4^{4-}$ monomer (corresponding to pH = 12.1 and pH = 7.1), two of the four nitrogen atoms in the core of porphyrin and the four sulfur groups are negatively charged. Due to large negative total charge (-4), it is unlikely that these monomers could form dimers. Only one H-dimer showed stable geometry, i.e., the geometry optimization has converged, where one of the monomers is rotated by 45° with respect to the other.

Figures 2(a) and 2(b) present the optimized $H_2TPPS_4^{4-}$ monomer and dimer from the top view, while Fig. S2(a) (see in the supplementary material) presents this dimer from the side view. We denote this dimer as $H_1^{(-)}$. The superscript denotes the overall negative charge of the structure. Figure S2 visualizes closely packed atoms that have possibly overlapping electron densities, thus signifying a strong electronic interaction. In the cases where these interactions are formed between benzene, benzene/pyrrole, and pyrrole rings, we denote such coordination as “ π - π stacking interaction”³⁷ throughout the text. Figure S2(a) shows that the $H_1^{(-)}$ dimer has one π - π stacking interaction between benzene rings.

The dihedral angle D (C_α , C_β , C_γ , and C_δ) was chosen to quantify the benzene group twist. It was found that benzene rings orient closer to the molecular plane in dimers than in the monomer since a perpendicularly oriented benzene ring could disturb the dimer formation. Dihedral angles of all converged configurations are

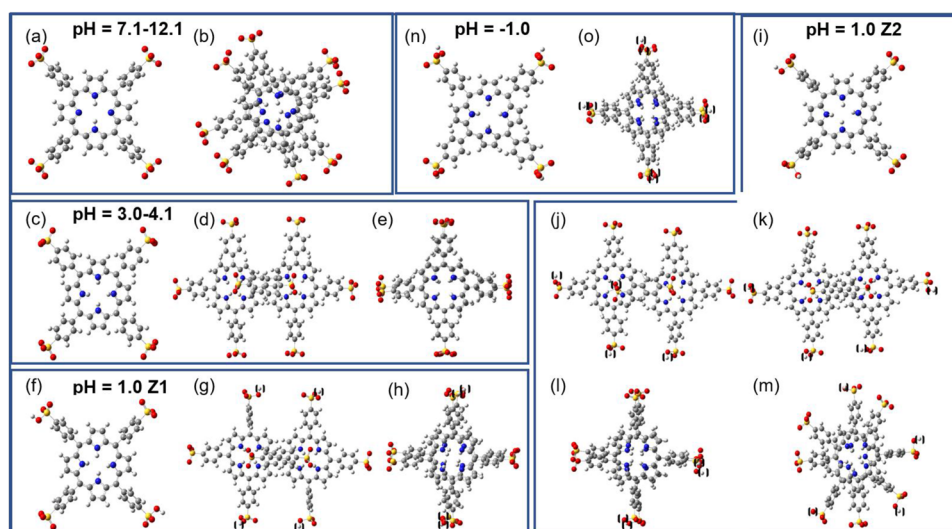


FIG. 2. Structures of $TPPS_4$ monomers and dimers (top views). (a) $H_2TPPS_4^{4-}$ monomer, (b) $H_1^{(-)}$ dimer, (c) $H_4TPPS_4^{2-}$ monomer, (d) $J_1^{(-)}$ dimer, (e) $H_2^{(-)}$ dimer, (f) Z1 monomer, (g) $J_2^{(0)}$ dimer, (h) $H_3^{(0)}$ dimer, (i) Z2 monomer, (j) $J_3^{(0)}$ dimer, (k) $J_4^{(0)}$ dimer, (l) $H_4^{(0)}$ dimer, (m) $H_5^{(0)}$ dimer, (n) $H_8TPPS_4^{2+}$ monomer, and (o) $H_6^{(+)}$ dimer. Hydrogens of SO_3H groups are marked by “(i)” in dimers.

presented in the supplementary material and are compared with the results obtained by Aydin.³⁸

In summary, the formation of aggregates is unfavorable at pH = 12.1 and pH = 7.1 at room temperature due to the total net charge, which is consistent with the literature.³⁹ Hence, $H_2TPPS_4^{4-}$ predominantly exists as a free-base monomer. This is confirmed by evaluating binding energies, which are smaller than the thermal energy (see the supplementary material). However, some dimerization may occur.

Structures based on the $H_4TPPS_4^{2-}$ monomer

All four nitrogen atoms of a $H_4TPPS_4^{2-}$ monomer are protonated. This form is typical for a pH range of 3–4. According to the structural symmetry, it could form one type of J-dimer and two types of H-dimers. The J-type dimer optimization did converge. However, only one structure of the H-dimer converged into a stable configuration, where molecules appear directly on the top of each other. Figures 2(c)–2(e), S2(b), and S2(c) present the optimized $H_4TPPS_4^{2-}$ monomer and corresponding dimers from the top and side views, respectively. We denote these dimers as $J_1^{(-)}$ and $H_2^{(-)}$. The $J_1^{(-)}$ dimer has one π - π stacking interaction between benzene rings [see Fig. S2(b)], whereas the $H_2^{(-)}$ dimer has five π - π stacking interactions between pyrrole and benzene rings [see Fig. S2(c)].

Structures based on the $H_6TPPS_4^0$ monomer

$H_6TPPS_4^0$ is denoted as the zwitterionic form of $TPPS_4$. This form dominates at a pH of ≈ 1 .^{13,26,27} This form of the molecule is neutral, so it is prone to aggregation. Two types of monomers can be formed: the “opposite” zwitterion, where two protons are placed on the opposite SO_3^- groups (we denote it by Z1), and the “adjacent” zwitterion, where two protons are placed on the adjacent SO_3^- groups (we denote it by Z2). The optimized structures of Z1 and Z2 monomers are shown in Figs. 2(f) and 2(i), respectively. It can be seen that the additional hydrogen do not significantly affect the entire molecular structure and only benzene rings corresponding to the protonated SO_3^- groups are rotated (twisted) more out of the plane of the porphyrin ring in the Z2 monomer.

The number of possible dimer configurations becomes large since outer hydrogens at different positions have different effects on the dimerization. This results in three J-type dimers and three H-type dimers; the structures are shown in Figs. 2(g), 2(h), and 2(j)–2(m). As in the previous case, the parameter characterizing the dimers is the relative binding energy. The binding energies of all converged zwitterionic dimers are listed in Table SII (see the supplementary material).

By considering inter-atomic distances between molecules in the dimers, it is found that the structure of the $J_2^{(0)}$ dimer has two π - π stacking interactions between the benzene rings and the pyrrole rings [see Fig. S2(d)]. However, four π - π stacking interactions are formed between the benzene rings in the $H_3^{(0)}$ dimer [see Fig. S2(e)]. The $J_3^{(0)}$ dimer has one π - π stacking interaction between the benzene ring and the pyrrole ring. The hydrogen bond appears between the H atom of the pyrrole ring and the O atom of the SO_3H group [see Fig. S2(f)]. The $J_4^{(0)}$ dimer structure contains five π - π stacking interactions between the H atom of the NH bond and the SO_3^-

group [see Fig. S2(g)]. In both these J^0 structures, hydrogen bonds are formed between the negatively charged sulfonate groups and the positively charged porphyrin ring, in accordance with the literature.²⁹ The $H_4^{(0)}$ dimer has one hydrogen bond between the O atom of the SO_3H group and the H atom of another SO_3H group [Fig. S2(h)]. The $H_5^{(0)}$ dimer has two π - π stacking interactions between the benzene ring and pyrrole ring [Fig. S2(i)].

Overall, both Z1 and Z2 monomers have the same absolute energy; thus, the interaction between different SO_3 groups is negligible. It was also noticed that D and D' dihedral angles have a larger variation in the Z2 monomer and its dimers than in the Z1 monomer and its dimers (see the supplementary material). The binding energies of molecules are still relatively small. However, due to structural diversity, the probability of dimerization becomes higher.

Structures based on the $H_8TPPS_4^{2+}$ monomer

The last group of structures that we consider corresponds to the dication form of $TPPS_4$ ($H_8TPPS_4^{2+}$) molecules (this form dominates in our experimental measurements at pH = -1.0). According to the literature, all four sulfonic groups of $TPPS_4$ are protonated at pH < 1.^{14,28} These structures form only one type of dimer, which we denote as $H_6^{(+)}$ [Fig. 2(o)]. J-dimers are not considered because all SO_3 groups are protonated and, thus, no additional electrostatic interactions are possible with the center of the other molecule in the dimer. The $H_6^{(+)}$ dimer has four π - π stacking interactions between pyrrole and benzene rings and also has one hydrogen bond between the O atom of the SO_3H group and the H atom of the other SO_3H group [see Fig. S2(j)]. Compared to room temperature thermal energy, the dimer is almost isoenergetic with monomers (see the supplementary material). Hence, the dimer formation is unlikely.

Absorption spectroscopy

Experimental results

Spectroscopy measurements were performed at very low concentrations of $TPPS_4$ molecules (Fig. 3). Under these conditions, we

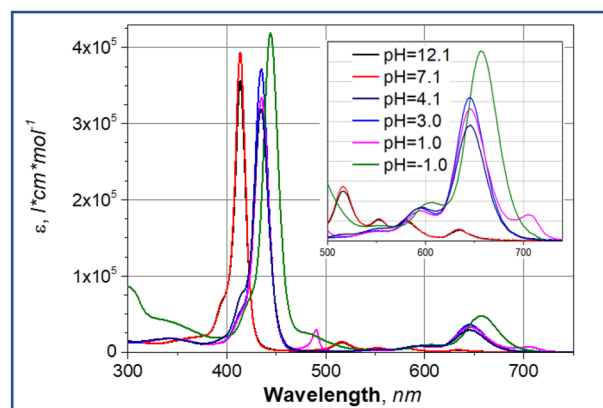


FIG. 3. Experimentally measured absorption spectra of $TPPS_4$ ($c = 3 \times 10^{-6}$ mol/l) at various pH values. The inset shows the enhanced Q band region.

expect mostly monomeric spectra to occur; however, the presence of some small aggregates in solutions at lower pH values should be possible. Formation of large aggregates should be ruled out.

In alkaline (pH = 12.1) and neutral (pH = 7.1) solutions, TPPS₄ molecules exist in a deprotonated (tetra-anion) form, possessing negative charges on four sulfonic residuals [H₂TPPS₄⁴⁻ Fig. 1(a)] and two protons at the porphyrin center. The TPPS₄ spectrum at these pH values is typical for etio-type porphyrins:⁴⁰ it has a B (the Soret) band with the major peak in the blue spectral region (around 413–414 nm) and four weak Q bands (between 516 and 635 nm) with relative intensities such that IV > III > II > I. Two out of the four bands are electronic transitions due to approximate C₄ symmetry. Accordingly, the other two peaks are related to the vibrational satellites. The band positions are listed in Table I. B and Q bands are marked by italicizing the corresponding spectrum peaks in the measured and theoretically calculated spectra. A weak blue-shifted shoulder of the main B band may be due to molecular vibrations.

The TPPS₄ pK_a value of protonation of nitrogen atoms at the porphyrin center is about 4.9 in a pure aqueous medium.⁵ Thus, a decrease in pH of the TPPS₄ solution from 7.1 to 4.1 and 3.0 favors binding of two protons to the central nitrogen atoms, creating a positive charge at the center of the porphyrin. This also leads to changes in the spectral pattern of TPPS₄ samples: from a four-band spectrum to a two-band spectrum in the Q region (at 595 and 645 nm) due to symmetry change (H₄TPPS₄²⁻) [Fig. 1(b)]. These changes also cause a bathochromic shift of the B band to 435 nm, while the band shape remains unaffected. These facts imply that Q-related transitions are localized on the porphyrin ring. Hence, adding two hydrogens changes the charge distribution and the

corresponding Q band spectrum considerably. The main electronic transition appears at 645 nm, while higher energy peaks resemble the vibrational progression. The B band essentially is not affected, and its shift originates mostly from the electrostatic Stark effect. Consequently, B band-related electron distribution may be mostly related to the periphery of the molecule.

A further decrease in the pH value to 1.0 leads to partial protonation of sulfonic (SO₃⁻) groups (two out of four) and formation of the zwitterionic form H₆TPPS₄⁰. The binding of two additional protons to SO₃⁻ groups cancels the negative charge, and the net charge of the TPPS₄ molecule becomes zero. The possible forms are displayed in Figs. 1(c) and 1(d). Protonation of two SO₃⁻ groups does not make a big difference on the features (positions of B and Q bands) of TPPS₄ absorption spectra, i.e., protonation of peripheral SO₃⁻ groups does not affect conjugated π-electron systems of the porphyrin ring. The position of the B band does not change (435 nm). There is a slight shift (by ~1 nm) in positions of Q and a new weak band appears at ~706 nm.

The zero net charge of the monomers presumably facilitates the formation of J-aggregate “seeds,” i.e., the J-type dimers. The appearance of a sharp absorption band at about 490 nm (we denote it as the J-band) and the second one at 706 nm could be attributed to dimerization and further oligomerization. Dimerization is additionally supported by the decay of the vibrational shoulder (compare the features of the main B-band at pH values of 1.0 and 3.0) due to exchange narrowing^{41–44} and hence renormalization of the vibrational features.

Decreasing the pH to extreme acidity (pH = -1.0) leads to protonation of all sulfonic groups (SO₃⁻) and formation of the dication

TABLE I. Experimentally measured and theoretically calculated positions of the main absorption peaks of TPPS₄ in aqueous solutions (c = 3 × 10⁻⁶ mol/l concentration).

| pH | Experimentally measured | | Theoretically calculated | | |
|--------------|-------------------------|---|--|-----------------------------------|---|
| | B (nm) | Q (nm) | Structure name | B (nm) | Q (nm) |
| 12.1 and 7.1 | <i>414^b</i> | 516, 552, <i>580^b</i> , <i>635^b</i> | H ₂ TPPS ₄ ⁴⁻ | <i>380^b</i> | <i>537^b</i> , <i>588^b</i> |
| | | | H ₁ ⁽⁻⁾ | 381^a , 399, 418 | 545, 595 |
| 4.1 and 3.0 | <i>435^b</i> | <i>595^b</i> , <i>645^b</i> | H ₄ TPPS ₄ ²⁻ | <i>398^b</i> | <i>634^b</i> |
| | | | J ₁ ⁽⁻⁾ | 399 | 622, 630 |
| 1.0 | <i>435^b</i> | <i>594^b</i> , 646^{a,b} | Z1 | 387 | 586, 599 |
| | | | Z2 | 389 | 585, 594 |
| | | | J ₂ ⁽⁰⁾ | 384, 396^a | 584 |
| | | | H ₃ ⁽⁰⁾ | 384 | 584, 601 |
| | | | J ₃ ⁽⁰⁾ | <i>400^b</i> | <i>609^b</i> , <i>617^b</i> , <i>627^b</i> , <i>633^b</i> |
| | | | J ₄ ⁽⁰⁾ | 390 | 589 |
| | | | H ₄ ⁽⁰⁾ | 383 | 586, 594 |
| -1.0 | <i>444^b</i> | <i>603^b</i> , <i>657^{a,b}</i> | H ₈ TPPS ₄ ²⁺ | <i>394^b</i> | <i>614^b</i> |
| | | | H ₆ ⁽⁺⁾ | 382 | 615, 626 |

^a Boldface denotes the strongest peaks of TPPS₄.

^b Italic denotes the peak wavelengths that correspond to the experimental results.

form ($H_8TPPS_4^{2+}$). This causes an additional shift of both B and Q bands roughly by the same spectral interval, presumably, due to the electrostatic Stark effect. A positive net charge (+2) causes electrostatic repulsion between monomers, which prevents aggregation, so the monomeric species (and the corresponding absorption characteristics) dominate. This is supported by the absence of the J-aggregate peaks in addition to the detected Q and B bands. However, there is still a notable broad shoulder in the 500 nm region, which may be related to “weak” disordered dimers.

TD-DFT calculations

The absorption spectra of various $TPPS_4$ ionic forms and the corresponding dimers were calculated for an interval of 350–700 nm encompassing both B- and Q-bands. The absorption spectra are presented in the form of extinction coefficient, ϵ , as a function of wavelength, λ . The spectra were normalized to compare the variation in the peak positions and the number of peaks in the same graph for monomers and dimers. A Gaussian band shape was added to the calculated stick spectrum with the full width at half maximum (FWHM) equal to 7 nm, for visualization purposes. The vibrational fine structure was not considered and, therefore, was not included in the spectra. No empirical rescaling of transition energies was introduced. Table I summarizes the theoretically calculated peak positions together with the experimentally measured data.

The calculated absorption spectra of the $H_2TPPS_4^{4-}$ monomer and the corresponding $H_1^{(-)}$ dimer are presented in Fig. 4(a). Peaks in the calculated absorption spectra were marked with the peak wavelength values (here and below, the peaks of the monomer are marked in blue, while peaks of dimers are marked in black). The spectral B region of the monomer shows much stronger absorption bands than those in the Q spectral region. The absorption peak of

the $H_2TPPS_4^{4-}$ monomer is at 380 nm in the B region, while two peaks are at 537 and 588 nm in the Q region. The $H_1^{(-)}$ dimer shows splitting of the spectral lines in the B region and a shift of absorption lines in the Q region. The peaks appear at 381, 399, and 418 nm in the B region, whereas Q bands are shifted to 545 and 595 nm.

The absolute peak positions in TD-DFT theory have systematic errors, so straightforward comparison to experiments should be avoided, and only a relative structure of the spectra, i.e., peak patterns, should be compared. Structures of B and Q bands being recorded experimentally at pH = 12.1 and pH = 7.1 are similar to the calculated spectrum of the $H_2TPPS_4^{4-}$ monomer. The vibrational side bands were not included in the calculations. Therefore, only one strong peak is observed in the B region (see Figs. 3 and 4). It confirms the prediction that monomers dominate at both pH = 12.1 and pH = 7.1 values. However, the calculated peak positions deviate from the experiment. In the B region, the shift is easy to define: the calculated peak is blue-shifted by 34 nm. Assuming wavelength rescaling by $380/414 = 0.91787$, we find that the theoretical peaks at 537 and 588 nm match the experimental peaks at 580 and 635 nm, respectively, thus suggesting that these peaks correspond to 0–0 electronic transitions. The experimental peaks at 516 and 552 nm can be attributed to the vibrational satellites.

At lower pH values of 3.0 and 4.1, a bathochromic shift of the B band by 21 nm becomes evident in the experimental spectra. The calculated absorption spectra of the $H_2TPPS_4^{2-}$ monomer and the corresponding $J_1^{(-)}$ dimer are presented in Fig. 4(b). By comparing the theoretical spectra of $H_2TPPS_4^{4-}$ (corresponding to pH = 12.1) and $H_4TPPS_4^{2-}$ (pH = 4.1), we also find the corresponding 18 nm shift of the B band for the monomer and for the dimer. The lowest energy Q band is shifted only 10 nm in the experiment. The shift in the Q region is very large (46 nm) in the calculated spectra. The spectrum of the $J_1^{(-)}$ dimer shows splitting of the Q band into two peaks separated by 8 nm. The spectrum of $H_2^{(-)}$ was not calculated because this dimer has positive binding energy and, therefore, is not stable (see Table SI in the supplementary material). The monomeric spectrum suggest that experimental peaks observed at 516 and 552 nm can be attributed to the vibrational origin since these features are not present in the calculated spectra.

For an even lower pH = 1.0 value, two SO_3 groups get protonated, which cancels the net charge of the molecule. The calculated absorption spectra of the $H_6TPPS_4^0$ monomer (Z1) and the corresponding $J_2^{(0)}$ and $H_3^{(0)}$ dimers made of this monomer, as well as those related to Z2 and its $J_3^{(0)}$, $J_4^{(0)}$, and $H_4^{(0)}$ dimers, are presented in Fig. 5.

The main peak of the Z1 monomer is at 387 nm (the peak consisted of two almost degenerate transitions at 385 and 391 nm) in the B region. Two 586 and 599 nm peaks are in the Q region. Similarly, the most intense absorption peak of the Z2 monomer is at 389 nm in the B region, while the Q region contains two peaks at 585 and 594 nm. The two monomers should be present at the same time, and they are indistinguishable by absorption spectroscopy. When comparing the modeling with the experimental spectra, the theory and experiment shows a single peak in the B region, while the structure in the Q band region is different: calculations show two peaks, while there is only one major peak (presumably single molecular) in the experiment. Note that the Q band peak splitting of the Z1 monomer

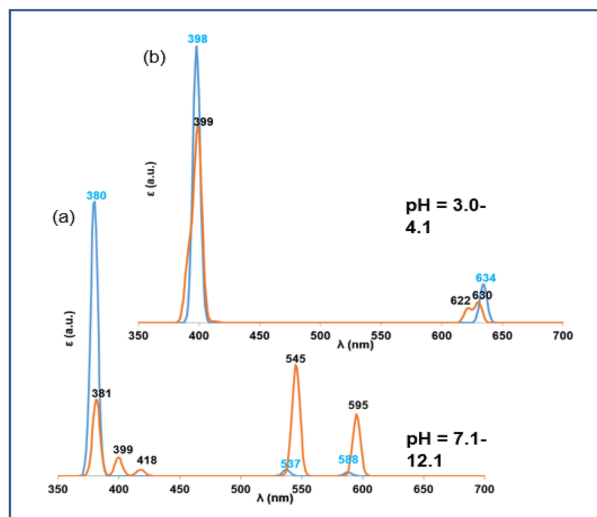


FIG. 4. Calculated absorption spectra of $H_2TPPS_4^{4-}$ and $H_4TPPS_4^{2-}$ monomers (blue lines) and $H_1^{(-)}$ and $J_1^{(-)}$ dimers (orange lines). (a) $H_2TPPS_4^{4-}$ monomer and $H_1^{(-)}$ dimer; (b) $H_4TPPS_4^{2-}$ monomer and $J_1^{(-)}$ dimer. Peak positions are marked with the peak wavelength value.

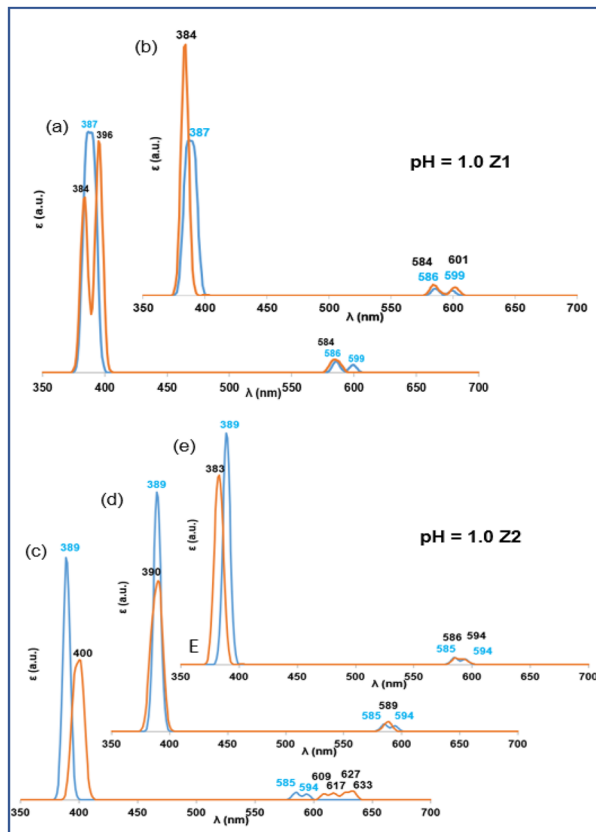


FIG. 5. Calculated absorption spectra of $H_6TPPS_4^0$ (Z1 and Z2) monomers (blue lines) and the corresponding dimers (orange lines): (a) Z1 monomer and $J_2^{(0)}$ dimer, (b) Z1 monomer and $H_3^{(0)}$ dimer, (c) Z2 monomer and $J_3^{(0)}$ dimer, (d) Z2 monomer and $J_4^{(0)}$ dimer, and (e) Z2 monomer and $H_4^{(0)}$ dimer. Peak positions are marked with the peak wavelength value.

is 13 nm while it is only 9 nm for the Z2 monomer. It turns out that, given the experimental results, these monomeric species contribute weakly to the measured spectrum.

We thus next switch to the dimers. The calculated absorption spectrum of the $J_2^{(0)}$ dimer [Fig. 5(a)] shows splitting of the B spectral line at 384 and 396 nm and merging of the Q transitions into a single 584 nm peak. The $H_3^{(0)}$ dimer has absorption peaks at 384 nm in the B region, as well as two 584 and 601 nm peaks in the Q region [Fig. 5(b)]. The $J_3^{(0)}$ dimer [see Fig. 5(c)] has a strong peak at 400 nm in the B region, and four peaks could be resolved in the Q region (at 609, 617, 627, and 633 nm). The spectrum of the $J_4^{(0)}$ dimer presented in Fig. 5(d) has the main peak at 390 nm, at almost the same position as in the spectrum of the Z2 monomer in the B region, and one peak at 589 nm in the Q region. Finally, the $H_4^{(0)}$ dimer [Fig. 5(e)] has the B peak at 383 nm and two Q peaks at 586 and 594 nm.

In summary, the modeling of spectroscopic features for Z1 and Z2 molecules points to the dominance of the $J_3^{(0)}$ dimeric form. This conclusion follows from the position of the B band observed in

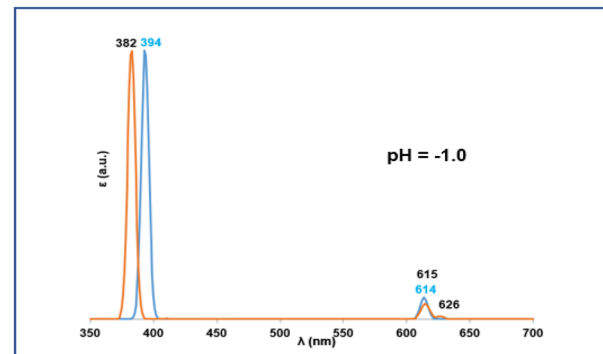


FIG. 6. Calculated absorption spectra of the $H_4TPPS_4^{2+}$ monomer (blue line) and $H_6^{(+)}$ dimer (orange line). Peak positions are marked with the peak wavelength value.

the calculations [Fig. 4(b)], which corresponded to the experimental spectrum (Fig. 3). This is also supported by the spectrum of Q bands, which, for the $J_3^{(0)}$ dimer, has a four-peak structure in the same region as seen in Fig. 4(b) and, again, corresponds well with the experimental data.

At pH = -1.0, the TPPS₄ molecule becomes a positively charged ion with all the protonated SO₃ groups. The calculated monomer spectrum (Fig. 6) has the strongest peak at 394 nm in the B region, whereas the peak in the Q region is at 614 nm.

The spectrum of the $H_6^{(+)}$ dimer has a peak at 382 nm in the B region and one peak at 615 nm with a shoulder at 626 nm in the Q band region. The peak in the B region becomes blue-shifted compared to that of the $H_8TPPS_4^{2+}$ monomer. The monomer spectrum pattern correlates with the experiment, showing one peak in the B region and one peak in the Q band region. Consequently, the monomeric form should be dominant in the solution.

DISCUSSION

The variability of the protonation pattern of TPPS₄ molecules with the pH value changes the electronic configuration of the molecule and correspondingly the optical properties as well as intermolecular interactions. Correspondingly, various types of molecular aggregates could be formed by changing the pH value with corresponding changes in the optical spectra. However, understanding the spectral properties of large molecular aggregates is challenging. The present study focuses on the variation in molecular spectra as a function of pH at low TPPS₄ concentrations, where formation of large molecular aggregates is unlikely. Instead, we should observe seeding elements, i.e., monomers and dimers.

An abundance of various dimers can be determined using relative energies of the monomers and dimers. For instance, when configurations A and B (both have the same number of atoms) having the corresponding energies E_A and E_B , respectively, are compared, the equilibrium populations of the configurations satisfy the statistical relation at temperature T as follows:

$$\frac{N_A}{N_B} = e^{-\frac{(E_A - E_B)}{k_B T}}, \quad (1)$$

where $k_B T$ is the thermal energy at temperature T , k_B is the Boltzmann constant, and N_A and N_B (E_A and E_B) are the number (density) of the species. This relation has to be adjusted when we compare separate molecules with the dimers (when the number of atoms is not the same for different configurations). Taking the absolute energy of the free molecule as E_0 , the absolute energy of the bound dimer is $2E_0 + E_b$. The absolute energy of the pair of molecules ($X + X$) is $2E_0$. Equation (1) thus reads $N_{XX}/N_{X+X} = S^{-1} \exp(|E_b|/k_B T)$. Here, S is the number of possible monomeric configurations, which is the entropic factor, related to the volume of the sample. For a pair of unbound molecules in the macroscopic sample, $S \gg 1$. For the binding energy $E_b \gg k_B T$, the molecules will form aggregates. The binding energies calculated for all structures studied are presented in the supplementary material. We found that all binding energies are quite small compared to the thermal energy (25 meV). Hence, when the dimers are formed, they dynamically dissociate and associate, and there is an equilibrium between various configurations. As a consequence, the statistical relation becomes obscure due to the unknown entropic factor. Hence, the experimental absorption spectra and their correspondence to the calculated spectra of various molecular configurations (monomeric and dimeric) become determinants and are used as the main evidence in determining the sequence of molecular changes as a function of pH.

The transformation sequence of molecular configurations obtained by changing the pH is shown in Fig. 7. The experimental spectra show that dimers are formed at pH = 1.0 and, most probably, they consist of the Z2 monomers. The main spectral signature appearing in the theoretical calculations of the dimers is a broad Q band covering the range of 605–640 nm, which extends down to 700 nm in the experimental spectrum. Notably, this molecular transformation sequence is roughly supported by both B and Q spectral bands. The B band gets red-shifted when the pH value is decreased from 7.1 to 4.1. Then it remains constant when decreasing the pH to -1.0. In contrast, the experimentally measured spectral band

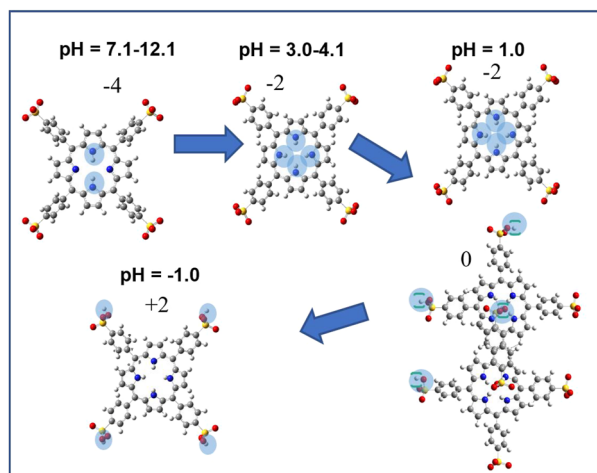


FIG. 7. Variation in the dominant TPPS₄ structure as a function of pH value. Positions of hydrogens are marked by blue shades. The total molecular charge is marked.

underwent a further bathochromic shift at pH = -1.0. The theory supports the spectral shift when changing the pH from pH = 7.1 to pH = 1.0; however, it cannot reproduce the further bathochromic shift by decreasing the pH to -1.0. Nevertheless, the H₄TPPS₄²⁺ monomer is “redder” than the corresponding dimer. It should be noted that the sharp peaks at 490 and 705 nm were not obtained in the calculations, suggesting that these features originate from the possibly formed larger aggregates.

It is important to point out the dynamic aspect of the protonation pattern. Protonation of SO₃ groups changes from no protonation at pH = 4.1 to full protonation at pH = -1.0. We showed that at pH = 1.0, Z1 and Z2 monomers had the same energy but their protonation pattern was different. The pattern of these hydrogens in the polar solution was fluctuating all the time, with protonation of SO₃ groups being defined on average. Momentarily, the proton distribution can be different. There is a notable experimental peak at 645 nm in the Q band region, which is dominant at pH = 4.1, 3.0, and 1.0. The peak should correspond to molecular monomers and, as shown by our analysis, is mainly attributable to H₄TPPS₄²⁻. Apparently, the solvent ions keep H₄TPPS₄²⁻ in dynamic balance with other ionic forms, and its presence is still highly probable at pH = 1.0. Notice also that experimental pH is the value corresponding to the whole volume. Molecules react to the nearby environment, which due to non-homogeneous distribution of ions and due to long-range Coulomb couplings may have local pH slightly different from the bulk. The zwitterion is then obtained by J₃⁽⁰⁾ dimerization, which causes broadening of a Q band and formation of the 705 nm band in the experiment. Apparently, dimerization is due to local changes in pH, and it causes local redistribution of charges in the environment. To match the experimental results, we must conclude that a free form of the zwitterion, most probably, is not observed.

Such results suggest that protonation–dimerization and local environmental ion redistribution is a feedback-driven adaptive problem. It creates local conditions quite different from the bulk (in terms of pH) due to the long-range Coulomb interaction between charged molecules and ions in the solvent.

The possible stable dimeric structures obtained in theoretical calculations for the charged molecules (tetra-anion, diacid, and dication form) were not expected due to the presence of the electrostatic Coulomb repulsion that should have destabilized the dimers. However, the most important factor in binding between molecules seems to be the interaction of benzene rings between the two molecules, which prevails the Coulomb repulsion. The situation is different for Z1 and Z2 monomers, where molecules are neutral but have well-expressed internal charged groups. It had been experimentally observed that TPPS₄ molecules aggregated efficiently into tubular structures at high molecular concentrations and a low pH value of around 1.^{7,45} The present study suggests the possible precursors of larger aggregates: the most probable aggregation seeder is the J₃⁽⁰⁾ dimer.

The zwitterionic forms are thus most important for large aggregate formation. The most intense absorption peaks of Z1 and Z2 monomers are found in the same higher energy region (387 and 389 nm, respectively). This demonstrates that the electronic states being responsible for the observed optical transitions were mostly localized on the main porphyrin ring. Outer benzene rings twist upon protonation (or deprotonation) of the SO₃ groups. Overall, this weakly affects the absorption spectra of molecules. The outer

benzene rings thus barely participate in transforming electron density on the porphine ring and affecting the spectra of B and Q bands.

There is a consensus that H-aggregates are characterized by a hypsochromic shift while J-aggregates are characterized by a bathochromic shift of the main absorption band.²¹ Therefore, these characteristics can be used as fingerprints when investigating the molecular structure of the aggregates. According to our results, the shapes of absorption spectra of monomers forming J and H dimers are not so trivial. Calculations showed that H-type structural dimerization did not introduce much perturbation to spectra compared to corresponding monomers. This indicates that intermolecular resonant interaction between the molecular transition charge densities becomes weak for H dimers. The result is different for J dimers, especially for $J_2^{(0)}$ and $J_3^{(0)}$. The Frenkel exciton model can be applied to model the spectra of such aggregates.

The most important question is related to the further growth of dimers into extended aggregates. The positioning of outer hydrogens (connected with sulfo-groups) must affect dimerization. First of all, large aggregates cannot grow from charged molecules (unless neutralized by solvent ions). We, thus, do not consider aggregation for tetra-anion, diacid, and dication forms. The neutral Z1 and Z2 monomers can grow into aggregates, keeping the overall neutral charge. Large aggregates also show the formation of tubular structures, which should correspond to some kind of bending of dimeric structures. According to our calculations, the aggregation is related to zwitterion formation, and the growth proceeds starting from Z2 monomers. This does not rule out the importance of the Z1 form. The Z1–Z2 dimerization is also possible, although it was not included in the present study. However, bending-kind formations in dimers were not obtained.

There is no consensus regarding whether the spectral hypsochromic shift (the B-band is at ~ 420 nm) is determined by π – π stacking interactions. Some authors conclude that this shift indicates the formation of H-aggregates in the solution. On the other hand, fluorescence detected linear dichroism microscopy and linear dichroism spectra of H_4TPPS_4 showed that the spectral bands at ~ 420 nm (usually characteristic of H-aggregates) and at ~ 490 nm (usually characteristic of J-aggregates) belong to the same structure.⁴⁶ Our results indicate the dominance of $J_3^{(0)}$ dimers at pH = 1.0. These results coincide with the literature reporting that $TPPS_4$ (in a form where a part of the peripheral SO_3^- groups is replaced by SO_3H) tends to form J-aggregates in acidified aqueous solutions because of the electrostatic repulsion being weakened between $TPPS_4$ molecules in the acidic solution (pH < 2).²⁷

It is important to point out that $TPPS_4$ absorption spectra were measured in aqueous solutions containing NaOH, HCl, or both (HCl and NaOH). Hence, the molecular environment was not pure water neither at pH = 7.1 nor at other pH values. The calculations were performed within the PCM approach of pure water. This theoretical model represents the charge distribution based on two separate areas, outside (solvent) and inside (solute) of a cavity,³¹ by describing them as a simple dielectric medium. The presence of Na ions in the $TPPS_4$ solution causes slight spectral shifts of absorption bands.⁴ The influence of diluted inorganic salts on the formation of aggregates can be studied with quantum mechanics/molecular mechanics (QM/MM) and molecular dynamics simulation, which will be a subject of further study.

CONCLUSIONS

The experimental absorption spectra of $TPPS_4$ solutions were studied at low concentrations in a broad range of pH values. Five $TPPS_4$ monomers and ten dimers that can be formed from these monomers at various pH values of the solvent have been studied by quantum chemical DFT calculations. The structures of monomers and dimers were determined and optimized. TD-DFT was used to calculate the absorption properties of $TPPS_4$ monomers and dimers, which were compared with the measured absorption spectra. The most sensitive spectral region of $TPPS_4$ molecules that could serve as a probe for changes in the microenvironment is that of the Q bands. A number of structural transformations of $TPPS_4$ have been determined when changing the acidity from pH = 12.1 to pH = –1.0. Based on our results, it can be said that the zwitterionic $J_3^{(0)}$ dimer formed at pH = 1.0 is one of the most likely candidates for the formation of large aggregates. At all other pH values, the corresponding monomers are expected to be dominant.

SUPPLEMENTARY MATERIAL

See the supplementary material for the initial (non-optimized) configurations of $TPPS_4$ dimers, the side view of the optimized dimers, and the calculated relative binding energies and dihedral angles of $TPPS_4$ monomers and dimers.

ACKNOWLEDGMENTS

This work was supported by the European Regional Development Fund, under Measure No. 01.2.2.-LMT-K-718 (Project No. 1.2.2.-LMT-K-718-02-0016), under a grant agreement with the Research Council of Lithuania (LMT-LT), and the Natural Sciences and Engineering Research Council of Canada (NSERC) (Grant No. RGPIN-2017-06923). Computations were performed on resources at the supercomputer “VU HPC” of Vilnius University in the Faculty of Physics location. The authors are grateful to Associate Professor Mindaugas Macernis for the helpful discussions.

AUTHOR DECLARATIONS

Conflict of Interest

The authors have no conflicts to disclose.

Author Contributions

Laura Baliulyte: Conceptualization (equal); Formal analysis (lead); Investigation (equal); Writing – original draft (lead); Writing – review & editing (equal). **Darius Abramavicius:** Conceptualization (equal); Supervision (equal); Writing – original draft (supporting); Writing – review & editing (lead). **Saulius Bagdonas:** Conceptualization (equal); Methodology (equal); Writing – original draft (supporting). **Agne Kalnaityte:** Conceptualization (equal); Investigation (equal); Methodology (equal); Writing – original draft (supporting). **Vilius Poderys:** Investigation (equal); Methodology (equal). **Ricardas Rotomskis:** Conceptualization (equal); Supervision (equal). **Virginijus Barzda:** Conceptualization (equal); Funding acquisition (lead); Project administration (equal); Supervision (equal); Writing – review & editing (equal).

DATA AVAILABILITY

The data that support the findings of this study are available from the corresponding author upon reasonable request.

REFERENCES

- ¹Q. Xiao, J. Wu, X. Pang, Y. Jiang, P. Wang, A. W. Leung, L. Gao, S. Jiang, and C. Xu, "Discovery and development of natural products and their derivatives as photosensitizers for photodynamic therapy," *Curr. Med. Chem.* **25**(7), 839–860 (2018).
- ²A. D. Schwab, D. E. Smith, B. Bond-Watts, D. E. Johnston, J. Hone, A. T. Johnson, J. C. de Paula, and W. F. Smith, "Photoconductivity of self-assembled porphyrin nanorods," *Nano Lett.* **4**(7), 1261–1265 (2004).
- ³N. C. Maiti, S. Mazumdar, and N. Periasamy, "J- and H-aggregates of porphyrin-surfactant complexes: Time-resolved fluorescence and other spectroscopic studies," *J. Phys. Chem. B* **102**(9), 1528–1538 (1998).
- ⁴L. P. F. Aggarwal and I. E. Borissevitch, "On the dynamics of the TPPS₄ aggregation in aqueous solutions: Successive formation of H and J aggregates," *Spectrochim. Acta, Part A* **63**(1), 227–233 (2006).
- ⁵I. G. Occhiuto, R. Zagami, M. Trapani, M. A. Castriciano, A. Romeo, and L. M. Scolaro, "Kinetic investigation on tetrakis(4-sulfonatophenyl)porphyrin J-aggregates formation catalyzed by cationic metallo-porphyrins," *Molecules* **25**(23), 5742 (2020).
- ⁶G. G. Parra, D. S. Correa, E. Silveira-Alves, Jr., L. M. Almeida, M. A. R. Souza, L. De Boni, L. Misoguti, C. R. Mendonça, S. C. Zilio, N. M. Barbosa Neto, I. E. Borissevitch, and P. J. Gonçalves, "Effects of meso-tetrakis (4-sulfonatophenyl) porphyrin (TPPS₄) aggregation on its spectral and kinetic characteristics and singlet oxygen production," *Spectrochim. Acta, Part A* **261**, 120063 (2021).
- ⁷M. Pleckaitis, F. Habach, L. Kontenis, G. Steinbach, G. Jarockyte, A. Kalnaityte, I. Domonkos, P. Akhtar, M. Alizadeh, S. Bagdonas, V. Karabanovas, G. Garab, R. Rotomskis, and V. Barzda, "Structure and principles of self-assembly of giant 'sea urchin' type sulfonatophenyl porphine aggregates," *Nano Res.* **15**(6), 5527–5537 (2022).
- ⁸J. M. Gottfried, "Surface chemistry of porphyrins and phthalocyanines," *Surf. Sci. Rep.* **70**(3), 259–379 (2015).
- ⁹M. O. Senge and M. Davis, "Porphyrin (porphine)—A neglected parent compound with potential," *J. Porphyrins Phthalocyanines* **14**(07), 557–567 (2010).
- ¹⁰H. L. Bonkovsky, J. T. Guo, W. Hou, T. Li, T. Narang, and M. Thapar, "Porphyrin and heme metabolism and the porphyrias," *Compr. Physiol.* **3**(1), 365–401 (2013).
- ¹¹M. Luciano and C. Brückner, "Modifications of porphyrins and hydroporphyrins for their solubilization in aqueous media," *Molecules* **22**(6), 980 (2017).
- ¹²M. W. Renner, M. Miura, M. W. Easson, and M. G. H. Vicente, "Recent progress in the syntheses and biological evaluation of boronated porphyrins for boron neutron-capture therapy," *Anti-Cancer Agents Med. Chem.* **6**(2), 145–157 (2006).
- ¹³T. Kim, S. Ham, S. H. Lee, Y. Hong, and D. Kim, "Enhancement of exciton transport in porphyrin aggregate nanostructures by controlling the hierarchical self-assembly," *Nanoscale* **10**(35), 16438–16446 (2018).
- ¹⁴J. M. Short, J. A. Berriman, C. Kübel, Z. El-Hachemi, J. V. Naubron, and T. S. Balaban, "Electron cryo-microscopy of TPPS₄·2HCl tubes reveals a helical organisation explaining the origin of their chirality," *Chem. Phys. Chem.* **14**(14), 3209–3214 (2013).
- ¹⁵Y. Zhong, J. Wang, and Y. Tian, "Binary ionic porphyrin self-assembly: Structures, and electronic and light-harvesting properties," *MRS Bull.* **44**(3), 183–188 (2019).
- ¹⁶K. Ishii, S. Hattori, and Y. Kitagawa, "Recent advances in studies on the magneto-chiral dichroism of organic compounds," *Photochem. Photobiol. Sci.* **19**(1), 8–19 (2020).
- ¹⁷R. Augulis, J. Tamulienė, A. Tamulis, and R. Rotomskis, "Theoretical modeling of TPPS₄ J-aggregates," *Solid State Phenom.* **97–98**, 225–228 (2004).
- ¹⁸S. C. M. Gandini, E. L. Gelamo, R. Itri, and M. Tabak, "Small angle X-ray scattering study of meso-tetrakis (4-sulfonatophenyl) porphyrin in aqueous solution: A self-aggregation model," *Biophys. J.* **85**(2), 1259–1268 (2003).
- ¹⁹B. A. Friesen, K. R. A. Nishida, J. L. McHale, and U. Mazur, "New nanoscale insights into the internal structure of tetrakis(4-sulfonatophenyl) porphyrin nanorods," *J. Phys. Chem. C* **113**(5), 1709–1718 (2009).
- ²⁰M. J. Hamor, T. A. Hamor, and J. L. Hoard, "The structure of crystalline tetraphenylporphine. The stereochemical nature of the porphine skeleton," *J. Am. Chem. Soc.* **86**(10), 1938–1942 (1964).
- ²¹T. Kobayashi, *J-Aggregates* (World Scientific Publishing Company, Singapore, 1996).
- ²²S. M. Vlaming, R. Augulis, M. C. A. Stuart, J. Knoester, and P. H. M. van Loosdrecht, "Exciton spectra and the microscopic structure of self-assembled porphyrin nanotubes," *J. Phys. Chem. B* **113**(8), 2273–2283 (2009).
- ²³A. Stradomska and J. Knoester, "Shape of the Q band in the absorption spectra of porphyrin nanotubes: Vibronic coupling or exciton effects?," *J. Chem. Phys.* **133**(9), 094701 (2010).
- ²⁴J. Valanciunaite, S. Bagdonas, G. Streckyte, and R. Rotomskis, "Spectroscopic study of TPPS₄ nanostructures in the presence of bovine serum albumin," *Photochem. Photobiol. Sci.* **5**(4), 381–388 (2006).
- ²⁵D. S. Correa, L. De Boni, G. G. Parra, L. Misoguti, C. R. Mendonça, I. E. Borissevitch, S. C. Zilio, N. M. Barbosa Neto, and P. J. Gonçalves, "Excited-state absorption of meso-tetrakisulfonatophenyl porphyrin: Effects of pH and micelles," *Opt. Mater.* **42**, 516–521 (2015).
- ²⁶U. Mazur and K. W. Hipps, "A systematic approach toward designing functional ionic porphyrin crystalline materials," *J. Phys. Chem. C* **122**(40), 22803–22820 (2018).
- ²⁷Y. Xiu, X. Zhang, Y. Feng, R. Wei, S. Wang, Y. Xia, M. Cao, and S. Wang, "Peptide-mediated porphyrin based hierarchical complexes for light-to-chemical conversion," *Nanoscale* **12**(28), 15201–15208 (2020).
- ²⁸M. A. Castriciano, A. Romeo, V. Villari, N. Micali, and L. M. Scolaro, "Structural rearrangements in 5,10,15,20-tetrakis(4-sulfonatophenyl)porphyrin J-aggregates under strongly acidic conditions," *J. Phys. Chem. B* **107**(34), 8765–8771 (2003).
- ²⁹G. Pescitelli, L. Di Bari, and N. Berova, "Application of electronic circular dichroism in the study of supramolecular systems," *Chem. Soc. Rev.* **43**(15), 5211–5233 (2014).
- ³⁰T. Yanai, D. P. Tew, and N. C. Handy, "A new hybrid exchange–correlation functional using the Coulomb-attenuating method (CAM-B3LYP)," *Chem. Phys. Lett.* **393**, 51–57 (2004).
- ³¹R. E. Skyner, J. L. McDonagh, C. R. Groom, T. van Mourik, and J. B. O. Mitchell, "A review of methods for the calculation of solution free energies and the modelling of systems in solution," *Phys. Chem. Chem. Phys.* **17**(9), 6174–6191 (2015).
- ³²R. Dennington, T. A. Keith, and J. M. Millam, GaussView, Version 6.1, Semichem Inc., Shawnee Mission, KS, 2016.
- ³³M. J. Frisch, G. W. Trucks, H. B. Schlegel, G. E. Scuseria, M. A. Robb, J. R. Cheeseman, G. Scalmani, V. Barone, G. A. Petersson, H. Nakatsuji, X. Li, M. Caricato, A. V. Marenich, J. Bloino, B. G. Janesko, R. Gomperts, B. Mennucci, H. P. Hratchian, J. V. Ortiz, A. F. Izmaylov, J. L. Sonnenberg, D. Williams-Young, F. Ding, F. Lipparini, F. Egidi, J. Goings, B. Peng, A. Petrone, T. Henderson, D. Ranasinghe, V. G. Zakrzewski, J. Gao, N. Rega, G. Zheng, W. Liang, M. Hada, M. Ehara, K. Toyota, R. Fukuda, J. Hasegawa, M. Ishida, T. Nakajima, Y. Honda, O. Kitao, H. Nakai, T. Vreven, K. Throssell, J. A. Montgomery, Jr., J. E. Peralta, F. Ogliaro, M. J. Bearpark, J. J. Heyd, E. N. Brothers, K. N. Kudin, V. N. Staroverov, T. A. Keith, R. Kobayashi, J. Normand, K. Raghavachari, A. P. Rendell, J. C. Burant, S. S. Iyengar, J. Tomasi, M. Cossi, J. M. Millam, M. Klene, C. Adamo, R. Cammi, J. W. Ochterski, R. L. Martin, K. Morokuma, O. Farkas, J. B. Foresman, and D. J. Fox, Gaussian 16, Revision C. 01, Gaussian, Inc., Wallingford, CT, 2016.
- ³⁴F. Würthner, T. E. Kaiser, and C. R. Saha-Möller, "J-aggregates: From serendipitous discovery to supramolecular engineering of functional dye materials," *Angew. Chem., Int. Ed.* **50**(15), 3376–3410 (2011).
- ³⁵M. Numata and R. Sakai, "Kinetically controllable supramolecular polymerization through synchronized activation of monomers," *Bull. Chem. Soc. Jpn.* **87**(8), 858–862 (2014).
- ³⁶Y. Zhao and D. G. Truhlar, "Density functionals with broad applicability in chemistry," *Acc. Chem. Res.* **41**(2), 157–167 (2008).
- ³⁷*Noncovalent Forces (Challenges and Advances in Computational Chemistry and Physics)*, edited by S. Scheiner (Springer, 2015).

- ³⁸M. Aydin, “Comparative study of the structural and vibroelectronic properties of porphyrin and its derivatives,” *Molecules* **19**(12), 20988–21021 (2014).
- ³⁹M. Li, L. Zhao, Y. Zhang, M. Liu, H. Ye, Y. Zhang, and X. Chen, “Adsorption behavior and self-aggregation of 5,10,15,20-tetrakis-(4-sulfonatophenyl)-porphyrin on quaternized polysulfone membrane,” *Colloid Polym. Sci.* **293**(2), 513–522 (2015).
- ⁴⁰L. B. Josefsen and R. W. Boyle, “Photodynamic therapy and the development of metal-based photosensitisers,” *Met.-Based Drugs* **2008**, 276109 (2008).
- ⁴¹F. C. Spano, “The spectral signatures of Frenkel polarons in H- and J-aggregates,” *Acc. Chem. Res.* **43**(3), 429–439 (2010).
- ⁴²M. Schröter, S. D. Ivanov, J. Schulze, S. P. Polyutov, Y. Yan, T. Pullerits, and O. Kühn, “Exciton–vibrational coupling in the dynamics and spectroscopy of Frenkel excitons in molecular aggregates,” *Phys. Rep.* **567**, 1–78 (2015).
- ⁴³A. Eisfeld and J. S. Briggs, “The J- and H-bands of organic dye aggregates,” *Chem. Phys.* **324**(2–3), 376–384 (2006).
- ⁴⁴M. Jakučionis, A. Žukas, and D. Abramavičius, “Modeling molecular J and H aggregates using multiple-Davydov D2 ansatz,” *Phys. Chem. Chem. Phys.* **24**(29), 17665–17672 (2022).
- ⁴⁵S. Chattoraj and K. Bhattacharyya, “Spatial inhomogeneity in spectra and exciton dynamics in porphyrin micro-rods and micro-brushes: Confocal microscopy,” *J. Chem. Sci.* **128**(11), 1717–1724 (2016).
- ⁴⁶Z. El-Hachemi, C. Escudero, F. Acosta-Reyes, M. T. Casas, V. Altoe, S. Aloni, G. Oncins, A. Sorrenti, J. Crusats, J. L. Campos, and J. M. Ribó, “Structure vs. properties — chirality, optics and shapes — in amphiphilic porphyrin J-aggregates,” *J. Mater. Chem. C* **1**(20), 3337–3346 (2013).